Available online at www.sciencedirect.com
ScienceDirect
Polymer 49 (2008) 999–1014
polymer
www.elsevier.com/locate/polymer

Investigation of the thermal, mechanical, and fracture properties of alumina–epoxy composites

Laura M. McGrath [a,b], Richard S. Parnas [a], Saskia H. King [b], John L. Schroeder [b], Daniel A. Fischer [c], Joseph L. Lenhart [b,*]

[a] University of Connecticut, Institute of Material Science, Polymer Program, Storrs, CT 06269, USA
[b] Sandia National Laboratories, Albuquerque, NM 87185, USA
[c] National Institute of Standards and Technology, Ceramics Division, Gaithersburg, MD 20899, USA

Received 21 May 2007; received in revised form 4 December 2007; accepted 9 December 2007
Available online 23 December 2007

Abstract

A combination of dynamic shear rheology, thermomechanical analysis (TMA), scanning electron microscopy (SEM), Near-Edge X-ray Absorption Fine Structure (NEXAFS), and fracture toughness testing was utilized to characterize the thermal, mechanical, chemical, and fracture properties of alumina (α-Al_2O_3)-filled epoxy resins as a function of average filler size, size distribution, particle shape, loading, and epoxy crosslink density. In general the cured properties of the filled composites were robust. Small changes in particle size, shape, and size distribution had little impact on the final properties. Resin crosslink density and filler loading were the most critical variables, causing changes in all properties. However, most applications could likely tolerate small changes in these variables also. SEM and NEXAFS characterization of the fracture surfaces revealed that the fracture occurs at the filler interface and the interfacial epoxy composition is similar to the bulk resin, indicating a weak epoxy–alumina interaction. These results are critical for implementation of particulate-filled polymer composites in practical applications because relaxed material specifications and handling procedures can be incorporated in production environments to improve efficiency.

Keywords: Epoxy; Composite; Filled polymer

1. Introduction

Since its first commercial production in 1947, epoxide-based (“epoxy”) materials have been used in a wide variety of products, such as adhesives, casting compounds, body solders, and encapsulates [1]. Good chemical resistance, excellent mechanical properties, and modification versatility make epoxy attractive, while its inherent low viscosity and volatility as well as moderate cure temperatures allow for production ease. The properties of epoxy can be tailored through a variety of monomer choices including aromatic, which provide stiff, high glass transition structural materials, and aliphatic, which can form elastomers. The molecular weight and molecular weight distribution as well as the chemical functionality of the monomers can be varied to provide further control over the properties. This chemical and processing flexibilities make epoxies useful in an array of applications including protective coatings, paints, adhesives, electronics, tooling, and composites.

Epoxies are commonly modified by the inclusion of inorganic-particulate fillers, such as silica [2,3], alumina [4–7], mica [8], or talc [9]. Fillers are added to epoxy resins to improve fracture toughness [10,11] and electrical or heat transfer properties [12,13], to increase resin stiffness [14], flame retardance [15], and wear resistance [4], and to reduce the coefficient of thermal expansion (CTE) [16]. The resulting composite specimens have applications as automobile parts

* Corresponding author. Sandia National Laboratories, Organic Materials, P.O. Box 5800 MS 0888, Albuquerque, NM 87185, USA. Tel.: +1 505 284 9209; fax: +1 505 844 9624.
E-mail address: jllenha@sandia.gov (J.L. Lenhart).

0032-3861/$ - see front matter © 2007 Elsevier Ltd. All rights reserved.
doi:10.1016/j.polymer.2007.12.014

[17], dental restoratives [18,19] and electronic packaging/underfill for circuit cards [20–22]. Many variables (*e.g.* resin crosslink density, particle type, size, size distribution, and filler loading) can affect the composite's thermal, electrical, mechanical and fracture properties. Rubber fillers increase fracture toughness with cracks propagating *via* cavitation and shear yielding phenomena, but decrease the flexural and Young's moduli [23,24], as well as increasing the CTE. Conversely, inorganic fillers typically provide an increase in modulus and a decrease in CTE, but do not provide as large of an increase in toughness compared to their organic counterparts [23].

While rigid inorganic particles are widely incorporated in epoxy or other polymer matrices, the micro-level fracture toughening mechanisms have not been firmly established [11]. In addition, the interactions between the inorganic particles and the matrix are poorly defined, as well as the impact of filler size, size distribution, and surface chemistry on failure mechanisms. From an application prospective, there is a need to understand the crucial variables and how these variables impact the composite properties, in order to establish material specifications as well as the sensitivity of the final device performance to these variables.

Alumina filled epoxy was chosen as the model system because of its prevalent use in electronic packaging [20–22] and dental restoratives [18,19]. The impact of the epoxy crosslink density, alumina loading, particle size, size distribution, and shape on the composite properties was explored. In particular, the composite fracture toughness, glassy and rubbery shear storage moduli, glass transition temperature, and glassy and rubbery CTE were investigated. Epoxies with two different crosslink densities ($T_g = 40$ and 82 °C) were employed. The basic chemistry of the two resins was kept constant, while the crosslink density was varied, by changing the molecular weight of the diamine hardener. The results in general show that the cured properties of the resin are insensitive to changes in the alumina characteristics, which is attributed in part to a weak alumina–epoxy interface.

2. Experimental [25]

2.1. Materials

2,2-Bis[4-(glycidyloxy)phenyl]propane (DGEBA, 348 g/mol, 97%) and polypropyleneoxide diamines (Jeffamine, $M_n = 230$ and 400, i.e. D230 and D400) were used as-received (Fig. 1) from Aldrich Chemical Company. α-Alumina corundum (AA2, AA5, AA10, AA18 from Sumitomo Chemical Co. Japan and T60 from Alcoa Co.) were dried in an oven at 110 °C under vacuum for at least 12 h prior to use. A Beckman Coulter Light Scattering particle size analyzer was used to determine the Al_2O_3 particle size and size distribution (Table 1). The chemically synthesized AA system, from Sumitomo Chemical Co., was chosen because of its narrow particle size distribution and nominal spherical geometry, whereas the milled T60 has a broader size distribution and a wide variety of jagged shapes (Fig. 2).

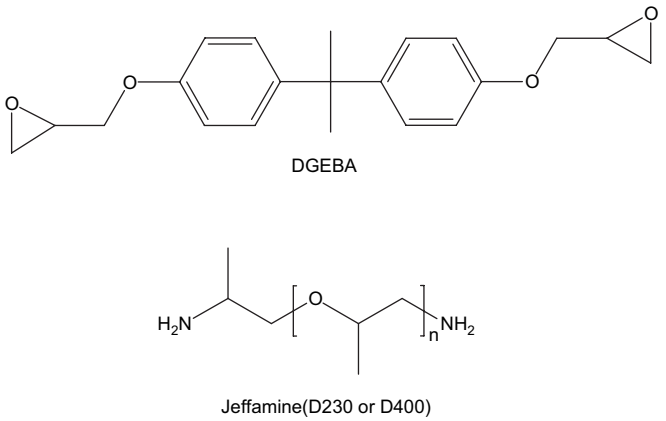

Fig. 1. Structure of epoxy monomers 2,2-bis[4-(glycidyloxy)phenyl]propane (DGEBA) and polypropyleneoxide diamines (Jeffamine D230 or D400).

2.2. Composite preparation

Both the epoxide and the diamine were preheated to 50 °C. Al_2O_3 was weighed to the appropriate vol.% (0–50) and placed in an oven at 75 °C. DGEBA and the respective diamine were mixed in a stoichiometric formulation, assuming that each amine hydrogen reacts with a single epoxy. The epoxide–amine mixture was placed in an oven at 75 °C for 15–45 min and was periodically stirred. After an initial viscosity increase that prevents the settling of powders, Al_2O_3 was added and mixed vigorously by hand to ensure proper particle wetting and homogeneity. The composite mixture was subsequently degassed at 55 °C. The viscous mixture was poured into preheated, release agent coated, aluminum molds. The resin in the molds was degassed and cured as follows: 25 °C, 2.5 h; 25–93 °C over 8 h; 93 °C, 3 h; 93–120 °C over 2 h; 120 °C, 2 h, and 120–25 °C over 2 h.

2.3. Characterization

Dynamic torsional shear experiments were conducted on a Rheometric Scientific ARES rheometer at a frequency of 1 Hz from 150 to −100 °C, at 2 °C/min in the respective linear strain regime of the sample. The CTE data were determined by thermomechanical analysis (TMA), (TA systems Q400), in accordance with ASTM E831. The sample was cycled four times from −60 to 150 °C at 2 °C/min and was held isothermal at each temperature limit for 10 min.

Fracture toughness single-edge notch (SEN) samples were prepared by cutting the composite into 63.5 mm long, 12.7 mm wide, and 6.35 mm thick sections. A razor blade was tapped into the center of the sample and a crack was propagated to a crack length equal to 20–80% of sample width, W.

Table 1
Al_2O_3 particle size and size distribution

Particle size (μm)	AA2	AA5	AA10	AA18	T60
Mean	3.683	5.064	8.083	16.700	18.81
Mode	3.359	5.064	8.536	18.000	26.14
Standard dev.	1.589	4.878	2.614	4.713	14.45

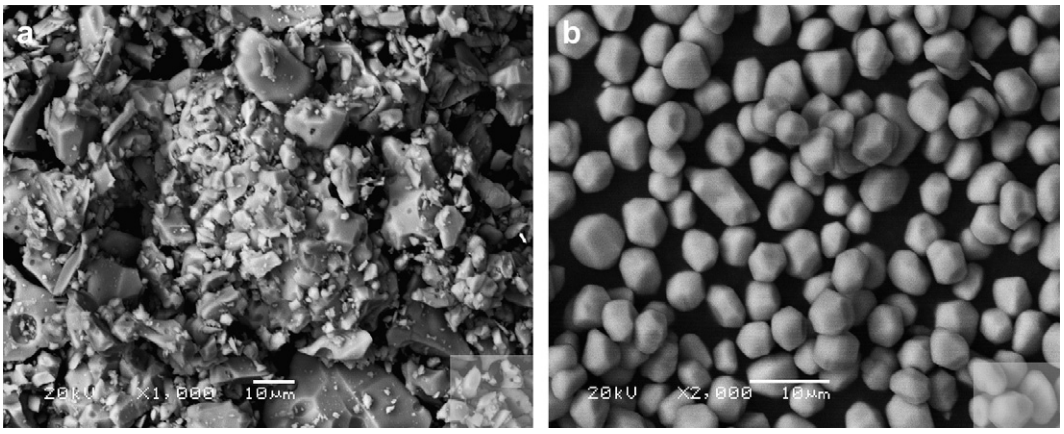

Fig. 2. SEM micrographs of Al_2O_3: (a) Alcoa T60 and (b) Sumitomo AA5.

The crack length, a, should be longer than the razor blade insertion, ideally twice as long. The ratio a/W should be between $0.45 < a/W < 0.55$. For the fracture toughness measurements, 5–10 samples were prepared from 1 to 3 sample sets. The SEN test was conducted in the three-point bend compression geometry (ASTM D1621) in an Instron Model 5589. A 1 kPa load cell with a 50.8 mm span was used at a crosshead speed of 6.35 mm/min. The samples were tested in the brittle regime, 40 °C below their respective T_g for each composite. All samples measured in this study maintained plane-strain conditions.

The fracture toughness test was used to calculate K_{Ic}, plane-strain fracture toughness (Eqs. (1) and (2)) where Y is the shape factor, P is the load to failure, S is the span of the Instron supports.

$$K_{Ic} = Y\frac{3PS\sqrt{a}}{2BW^2} \tag{1}$$

where

$$Y = 1.93 - 3.07\left(\frac{a}{W}\right) + 14.53\left(\frac{a}{W}\right)^2 - 25.11\left(\frac{a}{W}\right)^3 + 25.80\left(\frac{a}{W}\right)^4 \tag{2}$$

Note that the K_{Ic}, three-point bend fracture test, measures the state of stress around the crack tip and is used as a qualitative measure of toughness. It does not allow crack propagation to be studied. The sample must be thick enough so that the crack propagates without the sole energy release of the crack accelerating to the end of the sample. A continuous load versus displacement curve is observed in the load to failure curves during the three-point bending compression test.

Environmental scanning electron microscopic (SEM) studies of the fracture surface at 10–12 mm working distance and 20.0 kV were conducted in a Philips ESEM 2020. If charging occurred, the samples were coated with a 60:40 palladium/gold coating.

NEXAFS measurements were conducted at the U7A beamline of the National Synchrotron Light Source at Brookhaven National Laboratory. A monochromator, with 600 line/mm grating, provided ±0.15 eV resolution. The monochromator energy scale was calibrated by the carbon K-edge π^* transition of graphite at 285.35 eV. All the spectra were recorded at room temperature in the NIST – Dow material characterization chamber [26] at 10^{-6} Pa. The spectra were normalized to the incident beam intensity, I_0, by collecting the total electron yield intensity from a gold coated 90% transmitting grid placed in the incoming X-ray beam path. Surface sensitive partial electron yield measurements were made (probe depth of approximately 1–6 nm) by applying a negative bias on the entrance grid of the channeltron electron detector. The spectra were collected at the magic angle relative to the film surface to avoid orientation effects. For the NEXAFS spectra in this paper the experimental standard uncertainty in the peak position is similar to the grating resolution of ±0.15 eV. The relative uncertainty in the NEXAFS intensity is less than ±2% and was determined by multiple scans on a sample.

In NEXAFS, the sample is exposed to tunable, polarized, monochromatic X-ray radiation from a synchrotron light source. In these experiments, the incident radiation is scanned over the carbon (C1s) or oxygen (O1s) K-edge region, an energy range from 280 to 320 eV or 520 to 570 eV, respectively. X-Rays are preferentially absorbed by the sample when the incident radiation is at the appropriate energy to allow the excitation of a core–shell electron to an unoccupied molecular orbital. During electronic relaxation, Auger electrons and characteristic fluorescence photons are released. The electrons can only escape from the top surface of the sample, approximately 1–6 nm for these studies. The fluorescence photons were not collected in these experiments. NEXAFS has elemental sensitivity because the characteristic binding energies (carbon and oxygen core electrons) are well separated in energy. In addition, due to the well-defined energy gap associated with a core–shell/unoccupied orbital transition, NEXAFS is also sensitive to the bonding characteristics of the atom [27]. The NEXAFS spectra are pre-edge jump normalized (the background intensity before the respective C1s or O1s transition is subtracted) and post-edge jump normalized (the spectra

are normalized with the intensity in the post-edge region, leaving the post-edge with a value of 1 and allowing for direct comparisons of the chemical bonding).

3. Results and discussion

3.1. Rheology of filled and unfilled epoxy

3.1.1. Modulus versus temperature results

The shear storage modulus–temperature profiles are shown in Fig. 3a and b for the DGEBA/D230 and DGEBA/D400 composites, respectively, as a function of the vol.% loading of AA18 alumina. The storage modulus, in both the glassy and the rubbery regions, increases with increased filler loading. The characteristic drop of two to three orders of magnitude in G' represents the glass transition temperature. No appreciable change in the onset or midpoint of the glass transition temperature is detected as a function of filler loading. Fig. 3a and b also shows the loss tangent (tan δ or loss modulus divided by storage modulus) for the DGEBA/D230 and DGEBA/D400 systems. No appreciable shift in loss tangent maximum occurs with increasing filler loading. However, there is a subtle broadening of the glass transition region at the onset of the rubbery plateau region with increasing filler loading shown in both the tan δ and the storage modulus. This broadening is more prominent in the lower crosslink density DGEBA/D400 system. Potential causes of this broadening include particle–polymer interactions, particle–particle interactions, and particle agglomeration [28]. However, as will be discussed later, we hypothesize that particle–particle contact and the resulting friction are the causes.

In order to quantify the broadening effect, the inverse cumulative distribution function of the Lorentz distribution of the following form (Eq. (3)) was utilized to fit the data:

$$\log G' = \frac{1}{\pi} p1 \arctan\left(\frac{T - T_o}{\gamma}\right) + \frac{1}{2\pi} p2 \tag{3}$$

where T_o = temperature offset or glass transition temperature, γ describes the breadth of the transition, $p1$ is a scaling parameter, and $p2$ is an additional scaling parameter for temperature.

Fig. 4a and b shows fits of the modulus–temperature profiles over the glass transition region for the DGEBA/D230 system with 0 and 50 vol.% AA18 loading, respectively. Excellent fits were observed using Eq. (3), validating the utility for quantifying this broadening effect.

The resulting fitting parameters are shown in Table 2 for DGEBA/D230 and DGEBA/D400 with AA18 alumina. The curve broadening can be described by the γ parameter which increases with increasing vol.% of Al_2O_3. The T_g broadening is more pronounced in the DGEBA/D400 system. An increase in $p2$ with increasing vol.% Al_2O_3 also demonstrates the shift in onset of the plateau region to higher temperatures while not affecting the T_g, shown by the lack of change in the T_o value.

Broadening of the glass transition temperature has been observed for thin polymer films on silicon wafers [29] and loosely crosslinked thin epoxy films have been shown to exhibit glassy behavior at temperatures above the bulk polymer T_g [30,31]. In addition, a similar composite involving quartz powder in epoxy resin [28], the maximum value in tan δ associated with the α-relaxation, decreased with increasing filler vol.% and shifted to higher temperatures indicating a T_g increase. It was concluded that these results were due primarily to particle–polymer interactions. These reports [29–31] illustrate that the nature of the interface can impact the properties of the polymer in its vicinity.

The thermal properties of thin polymer films and polymers in interfacial regions are known to be different than the bulk. Both dewetting studies [32,33] and temperature dependent thickness measurements [34] have shown that polystyrene films can exhibit large scale mobility at temperatures well below the bulk polymer T_g. Subsequent research by a wide range of groups has shown that the properties of thin organic films can be different than the bulk and will depend strongly on the polymer–substrate interactions [29,35–50]. With strong polymer–substrate interactions, T_g can increase and the CTE

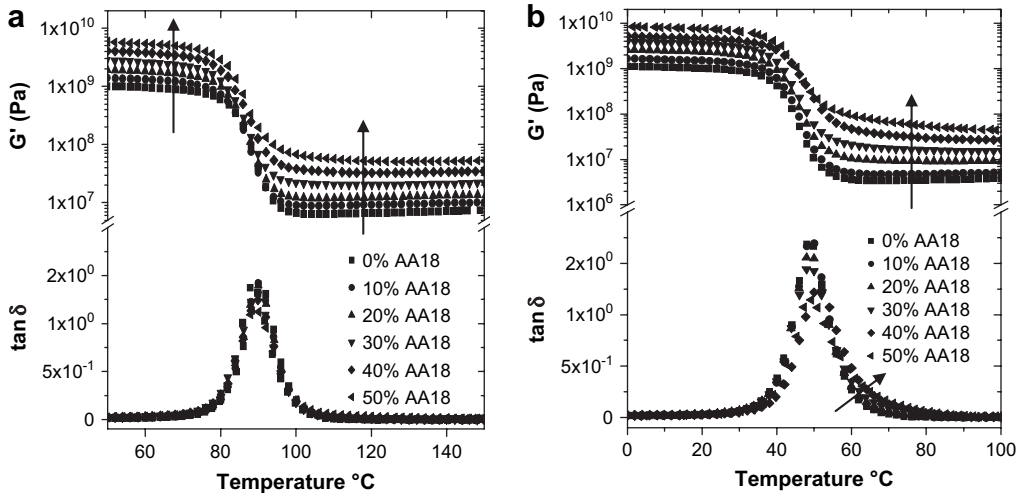

Fig. 3. Shear storage modulus and tan δ as a function of temperature for (a) DGEBA/D230 composites and (b) DGEBA/D400 composites; arrows indicate direction of increased filler loading.

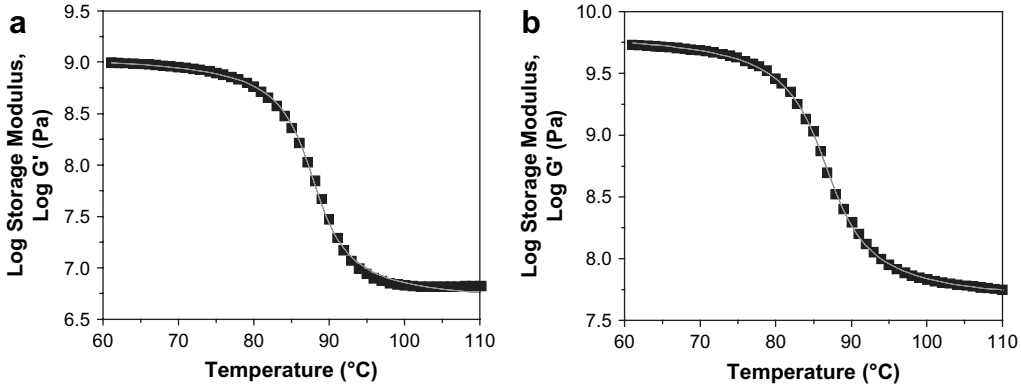

Fig. 4. Data fits for the DGEBA/D230 system with (a) 0% AA18 loading and (b) 50% AA18 loading. The line is the fit and the squares are the modulus data.

can decrease [35–42]. With weak polymer–substrate interactions, the T_g can decrease and the CTE can increase [35,36,39,41,43,44]. For free standing films, the T_g decreases dramatically [45]. These effects might be present at the buried epoxy–alumina interface in these composites. However, since no T_g increase was observed in these composites, it is likely that the epoxy–alumina interaction is not strong. Since the T_g does not decrease, the alumina–filler interface is also not behaving like a free surface, which is logical since resin shrinkage likely forces intimate epoxy–alumina contact.

Depending on the length scale of the interphase region a large change in the composite T_g may not be exhibited, regardless of the strength of the alumina–epoxy interaction. For example, due to the large size of the particles used in this study and their small surface area-to-volume ratio, a composite T_g change may not be observable with a small (i.e. sub 100 nm) interfacial region. In addition, various results have been reported for different alumina composites. For example, the glass transition has been observed to decrease in nano-alumina–poly(methylmethacrylate) composites due to poor polymer–filler adhesion [51], whereas epoxy composites filled with similar size alumina nanoparticles actually exhibited a slight T_g increase [52].

As will be shown later, the epoxy–alumina interaction is weak. Therefore we assert that the broadening is caused by the particle–particle contacts and the resulting friction. When slightly above T_g, particle–particle contacts may contribute to a readily observable increase in resin stiffness. When far above T_g, thermal expansion in the composite can reduce the friction from particle–particle contacts, with the combination of these two factors resulting in broadening of the modulus–temperature profile near but slightly above the T_g. The crosslink density affects the breadth of the α-transition in the epoxy–Al_2O_3 composites. The lower the epoxy crosslink density the greater the broadening, perhaps because the rubbery modulus is lower with the lower crosslink density resin leading to a more readily observable effect from particle–particle contacts. No change in broadening response with particle size was observed.

3.1.2. Alumina properties' effect on storage modulus

Fig. 5 presents the shear storage modulus (G') in the brittle regime (40 °C below T_g) and the rubbery regime (40 °C above T_g) for the epoxy composites as a function of alumina vol.% loading, filler type, and resin crosslink density. Similar to the observations in Fig. 3, the storage modulus increases with increasing filler vol.%, which is consistent with other epoxy systems where inorganic particles such as silica [53], glass [54–57], talc [9], and mica [8] were used. With increasing particle size (AA5, AA10, AA18, T60), there is no change in either the rubbery or the glassy modulus at each filler loading within experimental error. This was true for both crosslink density formulations. Comparison of T60 with AA18, which has similar average particle size but different size distribution and shape, indicates that particle size distribution and particle shape have no effect on the glassy or rubbery modulus of these composites.

Subtle changes in the flexural, compressive, and tensile moduli of glass filled epoxy composites have been observed as a function of average particle size [58–61]. However, the changes were hardly measurable over a range of particle sizes from 2 to 50 μm. For glass spheres in epoxy, Lewis and Nielson observed a small dependence of the relative shear modulus on particle size, but attributed it to a small resin-rich region on the sample edges [62]. Heikens and Vollenberg [63] found that when the interfacial adhesion between the particle surface and the polymer matrix is very good with covalent bonds present, the particle size altered the modulus. These studies corroborate the observations from these alumina–epoxy composites.

G' for DGEBA/D230 in the rubbery region is higher than that of DGEBA/D400, at each filler loading, indicative of the higher crosslink density. However, in the brittle region, the storage modulus of the D400 composite systems is slightly greater than that of the D230 system. This trend is interesting since previous work has shown that the crosslink density, monomer functionality, and chain stiffness have little impact on the glassy modulus or secondary relaxations of unfilled crosslinked epoxy resins [64].

Since the trend of higher glassy modulus with the D400 cured system is consistent at each filler loading, the subtle difference is real. Additional work is warranted with a broader range of epoxy crosslink densities, as well as chemical functionality, to determine the physical and chemical factors that are causing the differences in glassy modulus between the

Table 2
Fitting parameters for DGEBA/D230 and DGEBA/D400 with AA18 alumina

D230 AA18					D400 AA18				
Loading (%)	T_o	γ	$p1$	$p2$	Loading (%)	T_o	γ	$p1$	$p2$
0	87.83	3.51	−2.46	49.42	0	45.87	3.72	−2.77	48.7
10	87.31	3.53	−2.45	50.23	10	46.26	4.06	−2.87	49.52
20	87.34	3.70	−2.48	51.08	20	45.83	4.16	−2.7	51.24
30	86.70	4.11	−2.40	52.36	30	45.81	4.5	−2.6	52.69
40	86.94	4.40	−2.35	53.59	40	48.25	4.9	−2.44	53.96
50	86.71	4.29	−2.25	54.92	50	46.47	4.97	−2.34	55.66

D230 and the D400 systems. Other groups have attributed changes in the glassy region to hydrogen bonding [65] of the hydroxyl groups formed during the crosslinking reaction. Since the strength of a hydrogen bond decreases with increasing temperature, a lower crosslink density epoxy may form more effective hydrogen bonds in the glassy state at the same temperature relative to T_g. However, this explanation does not fit well with the observations in Fig. 5, because the glassy modulus for the unfilled DGEBA/D400 system is only slightly higher than that for the DGEBA/D230 system. Another potential explanation for the higher glassy modulus in the D400 composites compared to D230 is differences in particle–particle frictional effects in the two systems. The cure profile for both materials is the same, despite the differing ultimate T_g between the DGEBA/D400 and the DGEBA/D230 resins. Assuming resin shrinkage is proportional to the difference between the cure temperature and the final T_g, the DGEBA/D400 composites would exhibit more shrinkage during cooling from the cure temperature to room temperature, due to the increased CTE and decreased T_g of the DGEBA/D400 resin. As the filler loading increases, shrinkage can press the alumina particles against each other, increasing particle–particle friction. If the shrinkage is more prominent in the D400 composites, then the frictional forces may contribute more to the glassy modulus in that system compared to the D230 composites.

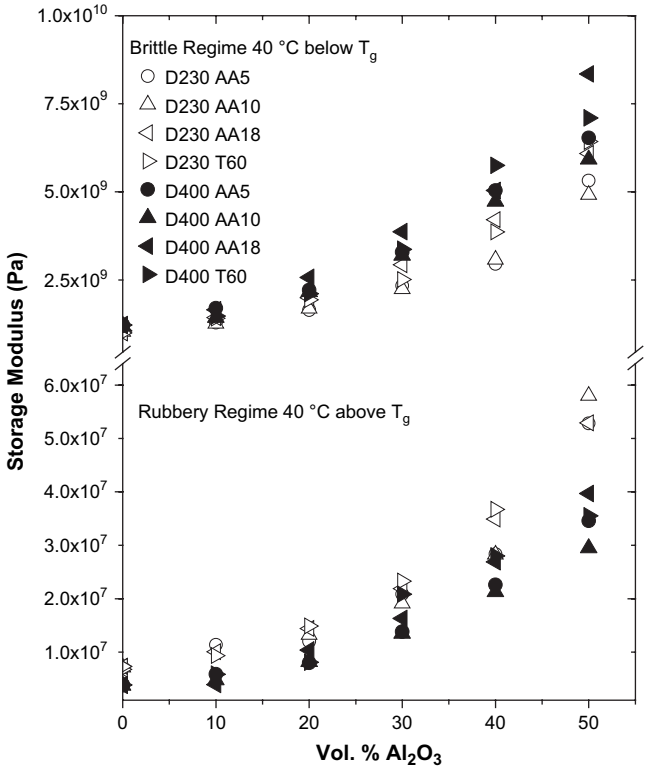

Fig. 5. (Top) the glassy modulus ($T_g - 40$ °C) for DGEBA/D230 (open symbols) and DGEBA/D400 (closed symbols) alumina composites as a function of alumina vol.%; (bottom) the rubbery modulus ($T_g + 40$ °C) for DGEBA/D230 (open symbols) and DGEBA/D400 (closed symbols) alumina composites as a function of alumina vol.% and particle type. The error is ±10% and was determined by multiple sample measurements.

3.1.3. Reduced modulus as a function of alumina

Fig. 6a and b shows the reduced modulus ($G'_{composite}/G'_{pure\ epoxy}$) for the DGEBA/D400 and DGEBA/D230 composites in both the glassy (40 °C below T_g) and the rubbery (40 °C above T_g) regions, respectively. The reduced modulus increase with increasing filler loading is more pronounced in the rubbery region, as has been observed with glass filled epoxy systems [10]. However, only subtle differences were observed in the reduced modulus between the D400 and D230 systems. The reduced modulus in both the glassy and the rubbery regions is independent of the average particle size, shape, and size distribution for the particles utilized in this study. For nanoparticle composites with high loadings, the reduced modulus may differ compared to larger particles due to particle–particle contacts, as nanoparticles are not readily dispersed in polymers.

Simple equations have historically been utilized to fit reduced modulus data. The Einstein equation was first proposed to describe the viscosity of rigid spheres in a liquid solution [66], and has since been a basis for describing a range of properties for two phase materials including modulus, thermal conductivity, and dielectric constant [67]. Guth proposed a quadratic expansion of the Einstein equation to describe various reduced properties in carbon black filled rubbers including the rubbery shear modulus [67]. More sophisticated equations, such as the Mooney equation (Eq. (4)), have also been utilized to describe the increase in relative viscosity of a suspension of dispersed spheres in solution as a function of filler volume fraction, and can be utilized to describe the increase in reduced modulus with filler loading. The Mooney equation accounts for the maximum packing fraction of particles in the matrix. However, it is only valid when Poisson's ratio is 0.5 (rubbery region) and the filler shear modulus is more than an order of magnitude higher than the polymer:

$$\frac{G'_{composite}}{G'_{epoxy}} = \exp\left[\frac{k_e \phi_f}{1 - (\phi_f/\phi_{max})}\right] \quad (4)$$

ϕ_{max} is the maximum filler packing fraction (approximately 0.63 for spherical particles) and ϕ_f is the actual particle volume fraction in the composite.

The Kerner equation (Eq. (5)) is also utilized to fit reduced modulus in both glassy and rubbery polymers and accounts for

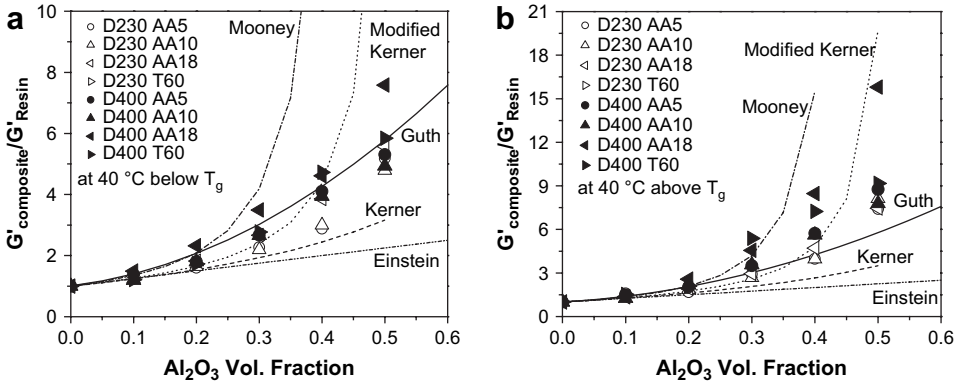

Fig. 6. The dependence of reduced modulus ($G'_{composite}/G'_{resin}$) of the DGEBA/D230 (open symbols) and DGEBA/D400 (closed symbols) composites on the alumina loading fraction and type in (a) the glassy region (40 °C below T_g) and (b) the rubbery region (40 °C above T_g).

changes in both Poisson's ratio in addition to the filler-to-polymer modulus ratio:

$$\frac{G'_{composite}}{G'_{epoxy}} = \frac{1+AB\phi_f}{1-B\phi_f} \quad A = \frac{7-5\nu_{epoxy}}{8-10\nu_{epoxy}} B = \frac{\left(G'_f/G'_{epoxy}\right)-1}{\left(G'_f/G'_{epoxy}\right)+A} \tag{5}$$

where ν_{epoxy} is Poisson's ratio for the pure epoxy resin and G'_f is the filler shear modulus. Improvements can be made by incorporating the effect of a maximum filler packing for a modified Kerner equation (Eq. (6)):

$$\frac{G'_{composite}}{G'_{epoxy}} = \frac{1+AB\phi_f}{1-B\psi\phi_f} \quad \psi\phi_f = \left[1+\left(\frac{1-\phi_{max}}{\phi^2_{max}}\right)\phi_f\right]\phi_f \tag{6}$$

Fig. 6a and b also shows data fits for the Einstein, Guth, Mooney, Kerner, and modified Kerner equations assuming an alumina shear modulus of 110 GPa and 0.63 as the maximum particle packing fraction. All equations provide a reasonable fit in both the glassy and the rubbery regions for filler volume fractions of 0.15 or less. Both the modified Kerner and the Guth expansions predict well in both the glassy and the rubbery regions up to about 0.4 filler fraction, which is consistent with observations with glass filled epoxy composites [62]. None of these equations provides great data fits especially at volume fractions greater than 0.4. However, these alumina particles are not monodisperse. Despite the well-defined nature of the Sumitomo alumina, they have a breadth to the size distribution (see Table 1). A broad size distribution will result in a larger maximum packing fraction than with monodisperse spheres, as small particles can fit into spaces around larger ones. Both the Mooney and the modified Kerner equations, assuming a larger maximum packing fraction, can provide better data fits up to 50 vol.% filler loading. A reasonable packing fraction of 0.7 is suitable for the modified Kerner equation. However, even larger assumed maximum packing fractions are required for the Mooney equation. Interestingly, both the Sumitomo particles and T60 show the same reduced modulus values (within experimental scatter), despite the widely different particle size distributions of the two.

3.1.4. Reduced modulus as a function of temperature

Fig. 7a and b plots the reduced modulus as a function of temperature for the DGEBA/D230 and DGEBA/D400 with AA18 alumina. In the glassy region the reduced modulus is independent of temperature for both resin systems, therefore the stress induced by the CTE mismatch between the epoxy and alumina is not large enough to move the resin into the non-linear region of the stress–strain diagram, as has been observed for silica filled epoxy resins [62]. Fig. 7 illustrates strong

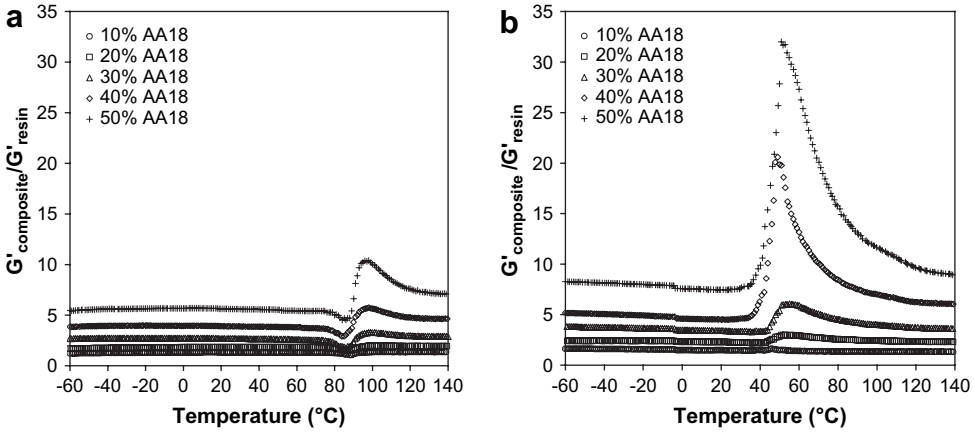

Fig. 7. The dependence of reduced modulus ($G'_{composite}/G'_{resin}$) with various AA18 volume loading percent in (a) DGEBA/D230 and (b) DGEBA/D400.

temperature dependence for the reduced modulus in the rubbery region with both the DGEBA/D230 and the DGEBA/D400 composites. The temperature dependence is more dramatic for the D400 composites, especially near the T_g. While this temperature dependence might be explained by a strong epoxy–alumina interface and the resulting broadening of relaxation times, the lack of a T_g shift in these composites suggests otherwise. Friction due to alumina–epoxy slippage at the interface is also not a likely explanation, since cure shrinkage with these composites promotes intimate polymer–filler contact. Our hypothesis again is that particle–particle friction is the cause of this broadening. While no agglomeration of alumina was observed in these composites, particle–particle contacts can still contribute to the composite stiffness and will be more prevalent at high filler loadings. In addition, the contribution of particle–particle frictional forces to the modulus would be more pronounced as the polymer modulus becomes less dominant (lower crosslink densities and in the rubbery region). Our hypothesis for particle–particle friction is supported by the observation that the maximum in reduced modulus as a function of temperature (just above T_g) starts to increase dramatically at filler volume fractions above 30%, which is typically associated with percolation phenomena in spherical particulates. However, more experiments are needed to verify this hypothesis including a broader range of epoxy crosslink density and filler size. In addition, an interesting approach would be to examine the impact of the particle–particle surface interactions and aspect ratio on the reduced modulus effect shown in Fig. 7. In higher aspect ratio fillers, percolation can be reached at much lower filler volume fractions than that for non-interacting spheres (~30 vol.%). Therefore, particle–particle contact and the resulting friction would become influential at lower filler loadings. This phenomenon might also be more prevalent with sub-micron to nanometer scale particles, where strong particle–particle interactions can lead to agglomeration and connectivity at smaller volume fractions. For the alumina utilized in this paper, thermogravimetric analysis (TGA) showed little mass loss even up to 900 °C, indicating that the particle surface is dry, and contained few surface hydroxyl groups. This was particularly prevalent with the Sumitomo particles, which exhibited no measurable mass loss in the TGA. Considering the lack of surface hydroxyl groups (which can generate a strong particle–particle surface interaction) combined with the large particle sizes, it is unlikely that the alumina filler utilized here is exhibiting connectivity at low filler volume fractions. In addition, the scanning electron microscopic images in Fig. 10 show directly that the alumina particles do not aggregate. With nanoscale particles or particles that have stronger attractive surface chemistries (i.e. carbon black or silica) this aggregation/connectivity could be an important phenomenon that impacts the composite modulus at smaller volume fractions.

3.2. Coefficient of thermal expansion (CTE)

The coefficient of thermal expansion (CTE) is a critical variable for epoxy composites in electronic packaging. The CTE for the brittle and rubbery regions is shown in Fig. 8a and b for the DGEBA/D230 and DGEBA/D400 composites, respectively, as a function of filler loading and filler type. The lines represent the CTE values that would be obtained with a rule of mixtures (ROM) prediction. The decrease in the rubbery or glassy CTE was independent of the average particle size, size distribution, and shape for both crosslink density systems. In the rubbery region, the CTE decrease follows the ROM closely. This is also consistent with a weak epoxy–alumina interfacial region as the thin film polymers' research typically shows a decrease in a rubbery CTE with strong polymer–substrate interactions. In the brittle regime, the CTE decrease deviates slightly from ROM. This deviation from rule of mixtures has been observed in filled systems and can be predicted with various types of empirical fitting [10].

3.3. Fracture toughness of alumina–epoxy composites

3.3.1. Particle size and distribution effects on the toughness of epoxy–Al_2O_3

Fig. 9a and b shows the fracture toughness for the DGEBA/D230 and DGEBA/D400 composites, respectively, as a function of filler size, filler shape, and filler loading. For both systems the fracture toughness of the composites increases with increasing filler loading. No trend with fracture toughness on particle size was observed in either resin systems. In addition, no impact of filler shape was observed as both Sumitomo (AA2, AA5, AA10 and AA18 nominally spherical) and Alcoa (T60 odd shaped) showed similar fracture toughness values at each filler loading. Similar results have been observed in silica filled epoxy resins. For example, no differences in fracture toughness were observed for small (~3 μm) and large (~25 μm) glass beads in crosslinked epoxy resins [68]. In addition, silica filled epoxies showed no substantial changes in fracture toughness over a particle size range of 60–300 μm at 40 vol.% loading [69]. The dependence of fracture toughness on average particle size has been explored for both angular [70] and spherical [71] silica particles in epoxy resin at filler loadings near 35 vol.% (55 and 64 wt%). A small decrease (approximately 20–40%) in fracture toughness was observed with decreasing particle size over a range from 2 to 50 μm. However, no particle shape effect was observed as both spherical and angular particles showed similar toughness values. More extreme variations in filler aspect ratio have been shown to impact fracture toughness in epoxy resins as short glass fibers (aspect ratio of 15) show substantially higher fracture toughness than glass beads (aspect ratio of 1) [69]. The toughness difference between non-spherical silica particles and glass beads was less significant [69].

Some researchers have observed a maximum in fracture toughness at an optimal particle loading [57,72]. This has been attributed [23] to the effect of inter-particle spacing. As the inter-particle spacing becomes smaller, it is more likely that micro-cracks will be generated that will act as stress concentrators ahead of the crack tip. For these alumina composites no maximum in fracture toughness with filler loading was observed. The changes in the particle size distribution did not have an effect on the fracture toughness, as there were no changes in K_{Ic} values of the T60 system compared to the

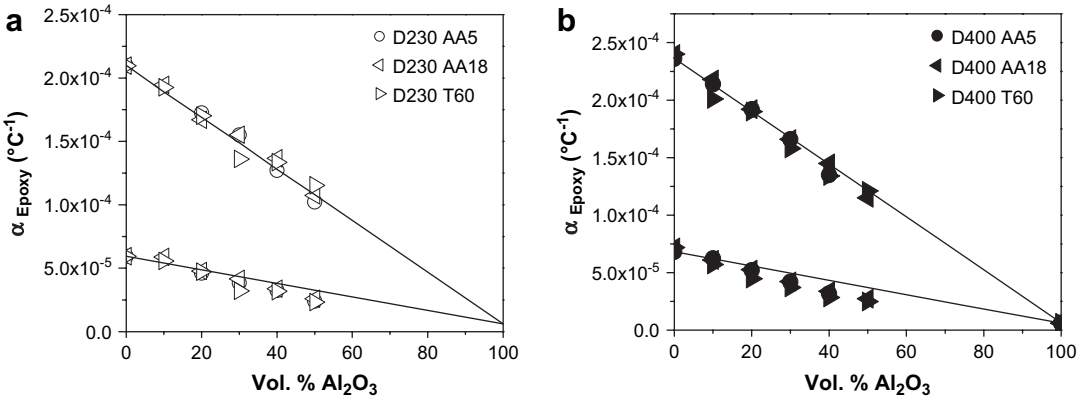

Fig. 8. The coefficient of thermal expansion as a function of the vol.% of Al_2O_3 in (a) DGEBA/D230 and (b) DGEBA/D400 with various particle sizes (lines represent the theoretical rule of mixtures).

AA system, thus concluding that the particle packing in these samples did not alter the composite toughness.

3.3.2. Effect of increase of diamine spacer length on composite toughness

One interesting effect in Fig. 9 is the impact of the epoxy crosslink density on the composite fracture toughness. Considering all the filler sizes and types collectively, the DGEBA/D400 composites showed higher fracture toughness values compared to the DGEBA/D230 composites. While this difference was subtle ($\sim$10 to 30% change as filler loading increases) and the data spread is fairly large, it occurred at each filler loading, despite the fact that the fracture toughness for each system was measured at the same temperature relative to the composite T_g ($T_g - 40$ °C). The mechanism responsible for fracture in unfilled epoxy resins is plastic deformation at the crack tip [73,74]. An increase in unfilled matrix toughness might be expected as the epoxy crosslink density decreases [73]. However, no fracture toughness difference was observed between the unfilled DGEBA/D400 and DGEBA/D230. While the exact cause of the higher fracture toughness in the D400 composites is unclear, a potential mechanism is that enhanced cure shrinkage in the D400 system (due to the lower T_g and higher rubbery CTE) leads to more effective crack pinning during fracture in composites with a weak polymer–filler interaction. More research is required utilizing various resin cure cycles to verify this hypothesis.

Fracture mechanisms in inorganic particle filled polymer composites have traditionally been described by the crack-front bowing theory [1,75,76,77]. Originally proposed by Lange [76], energy dissipation is increased by the rigid inorganic particles because the crack front needs to bow or move around the particle, yet as the crack encounters a particle it remains pinned to it. Energy is required to generate the increased crack length, thus, changing the particle size, shape, and volume loading can alter the energy required to propagate the crack front [78–80]. Typically with crack bowing, a step defect is observed in the fracture surfaces due to the fact that the crack front moving around each side of the particle does not meet perfectly once past the inclusion. Fig. 10a clearly shows these step defects in a 10 vol.% AA18 loaded DGEBA/D230 composite, as the bright tails behind the particles at the small filler loadings. Tails [23,57,76] or ridges in the epoxy are observed in the fracture surface below an Al_2O_3 particle in the crack front (Fig. 10a). This is a direct conformation that crack-front bowing is occurring. If the alumina–epoxy interface is poor, the Al_2O_3 will still divert the crack and toughen the material, but a weak interface without covalent bonds might limit the achievable toughening. This is corroborated with Green et al. [80,81] who found that with low interfacial adhesion the particles cannot pin the crack front and offer little

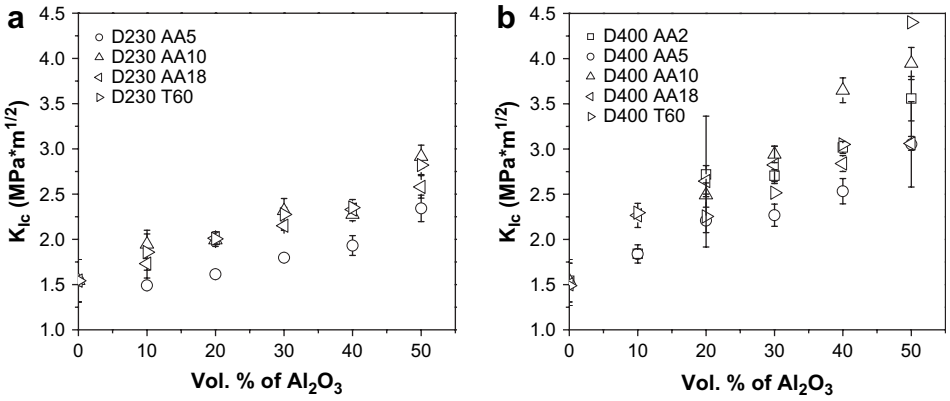

Fig. 9. Fracture toughness as a function of filler loading and filler type for (a) DGEBA/D230 composites and (b) DGEBA/D400 composites.

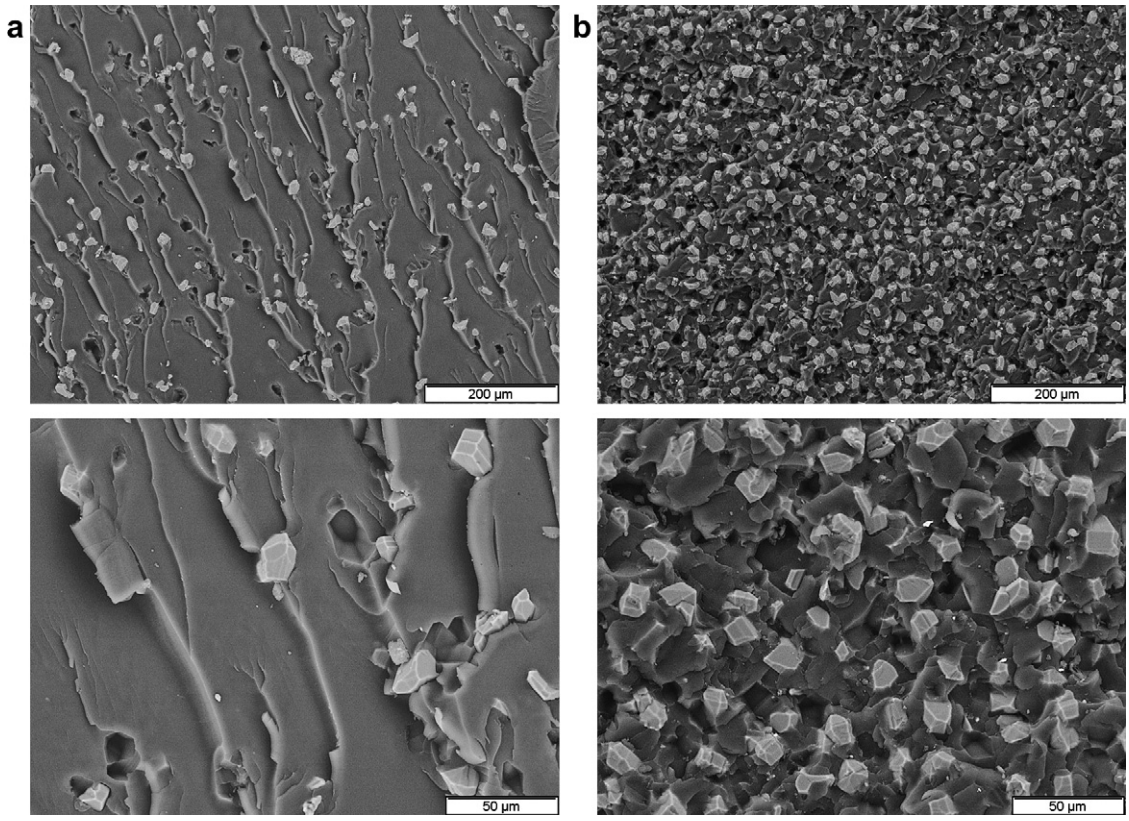

Fig. 10. SEM images of fracture surfaces in the processing zone for (a) 10% AA18 and (b) 50% AA18 loading both in DGEBA/D230. Top images are at a magnification of 150×. Bottom images are at 500×.

resistance. Both Fig. 10a and b shows that the fracture occurs at interface between the alumina and the epoxy, indicating weak adhesion. Fig. 10b shows the fracture surface for a 50 vol.% loaded alumina composite. Even at 50 vol.% loading, the alumina particles are well dispersed.

A broader range of particle sizes, particle–particle interactions, and particle–particle contact might reveal an interesting impact on the fracture toughness, and is a focus of ongoing investigations. Assuming the validity of the crack pinning model, we speculate that sub-micron size particles should exhibit enhanced fracture toughness when compared to larger particles at the same volume fraction loading, because more sub-micron particles will be present in the composite, presenting more sites for crack pinning. However, one challenge with sub-micron particulates is dispersion in the resin. Particle–particle interactions can lead to agglomeration and connectivity of the nano or sub-micron particles at lower filler volume fractions. The SEM images show that the alumina particulates in these composites are well dispersed with no observable agglomeration. With smaller size fillers or fillers with strong surface chemistry leading to substantial particle–particle connectivity, we speculate that micro-cracking phenomena could be more prevalent, especially if the resin poorly wets the particle at the particle–particle contacts. Perhaps this contributes to why some researchers have observed a maximum in fracture toughness at intermediate filler loadings with glass fillers, with a subtle decrease in fracture toughness at high filler loadings. Glass–silica particles typically have a high surface hydroxyl content, which could lead to enhanced particle–particle connectivity in these composites, making them more susceptible to micro-cracking phenomena.

Fig. 9 shows a subtle increase in fracture toughness with decreasing crosslink density. This fracture toughness increase was demonstrated over all filler loadings from 0 to 50 vol.%. Yee and Lee [73] also showed that the crosslink density of the polymer matrix had an impact on the fracture toughness of the composite. They attributed this to the toughness changes intrinsic in the unfilled polymer matrix with decreasing crosslink density. As the crosslink density decreased the unfilled matrix toughness increased and the resulting composite toughness increased. While this is expected, the interesting observation was that the filler incorporation was more effective in improving toughness as the crosslink density decreased [73]. While they only tested a single filler volume loading of 10%, this result is in contrast to traditional thought in the field that the toughening effect of filler incorporation in the polymer decreases as the intrinsic matrix toughness increases (i.e. the filler is not as effective in improving toughness in matrices that are already tough). The data in Fig. 9 show that the unfilled DGEBA/D230 and DGEBA/D400 polymers exhibit similar fracture toughness values. Therefore, a change in the intrinsic matrix toughness does not explain the crosslink density effect observed in Fig. 9. A pertinent question is whether the impact of the unfilled matrix toughness on composite toughness is generalizable with different crosslinking systems.

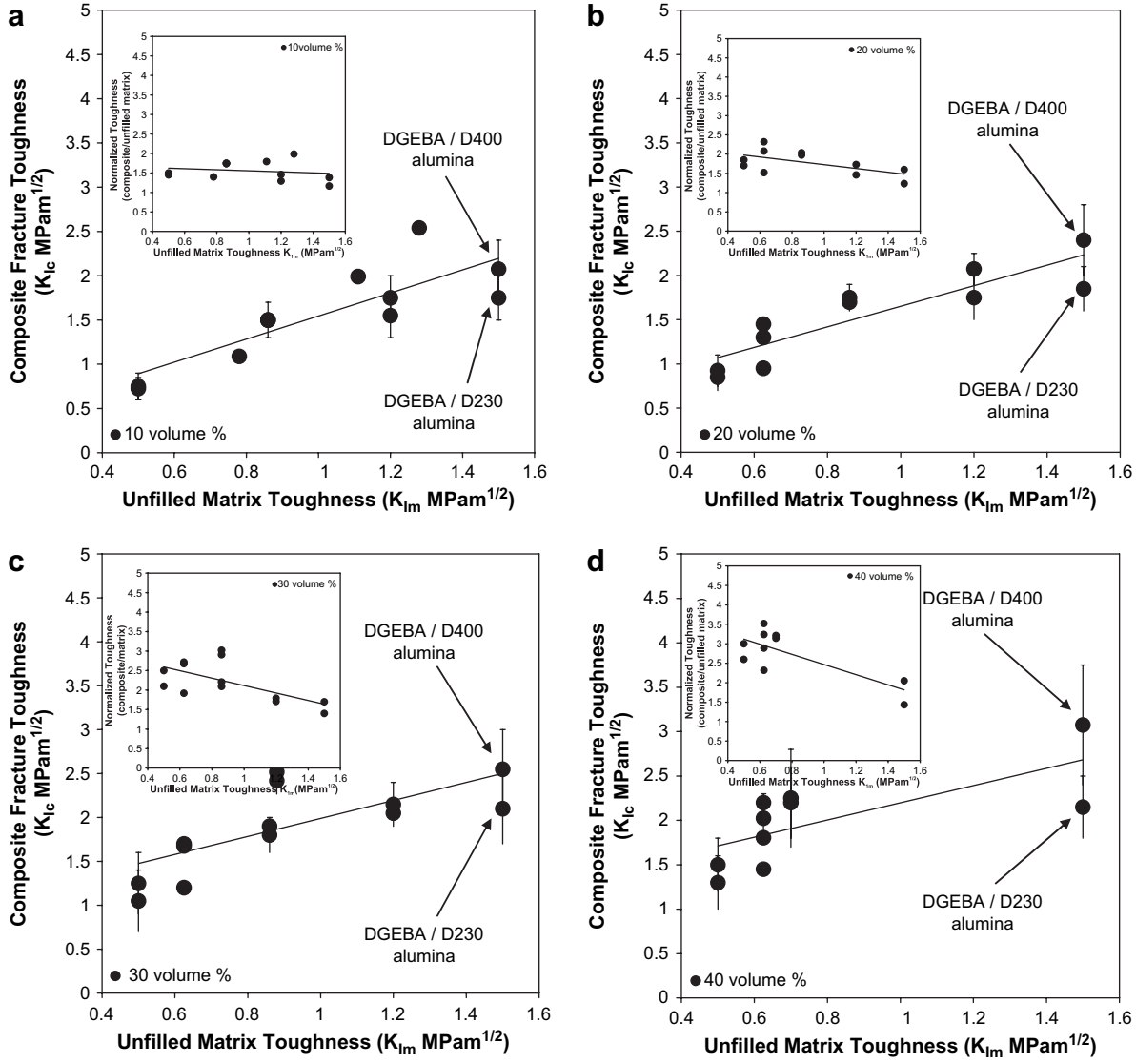

Fig. 11. Fracture toughness of particulate-filled composites as a function of the toughness of the unfilled matrix, for various filler volume fractions (a) 10%, (b) 20%, (c) 30%, and (d) 40%. Data take from Refs. [23,57,68–71,73,74,82,83]. The lines in the figures and the inset represent the best fits to the data.

Fig. 11 shows the summary of fracture toughness data as a function of the unfilled matrix toughness for a variety of different crosslinked epoxy systems that have been published in the open literature, including the alumina loaded composites for this report. The composites were composed of various epoxy resins and fillers. The fillers utilized in Fig. 11 include both silica and alumina. In addition, data for both spherical fillers and odd-shaped ''angular'' fillers are included as well as fillers with different sizes ranging from a few microns to several hundred microns. Also, the data in Fig. 11 are a combination of single-edge notch testing and dual torsion bar testing. However, these different testing methods have generally been shown to give similar results. The data for the unfilled matrix toughness equal to 1.5 MPa $m^{1/2}$ are the alumina–epoxy fracture toughness data from this report. A couple of interesting points are noted in Fig. 11. First, for the alumina composites in this paper, the fracture toughness of the DGEBA/D400 system is higher than the DGEBA/D230 system at each filler loading just as stated in Fig. 9. Second, a general trend was observed with each filler loading: as the intrinsic toughness of the unfilled matrix increases, the composite toughness increases. This makes physical sense, since the crack is propagating through the matrix material. Therefore, improvements in energy dissipation and crack resistance in the unfilled matrix will translate into improvement in the composite fracture toughness. The insets, for each filler loading, show the normalized composite fracture toughness (*Y*-axis, composite toughness/unfilled matrix toughness) as a function of the unfilled matrix toughness (*X*-axis). While the trend is subtle, the insets clearly support conventional wisdom: as the unfilled matrix toughness increases, the improvements in toughness upon filler incorporation decrease. This indicates that the conclusions of Yee and Lee [73] are not general within epoxy-based resin systems. Additional experimentation is warranted to investigate the impact of resin crosslink density and matrix toughness.

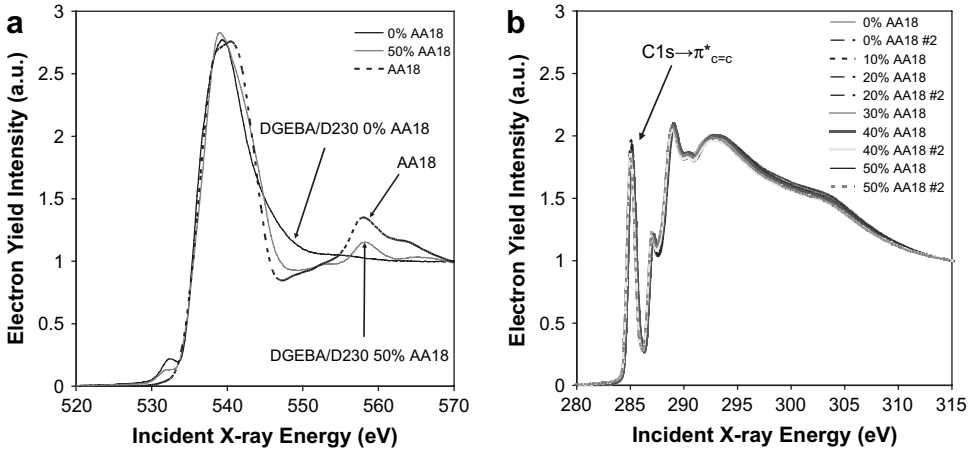

Fig. 12. NEXAFS spectra of the fracture surfaces for the DGEBA/D230 composites with various loadings of AA18 over (a) the oxygen *K*-edge and (b) the carbon *K*-edge. Similar results were observed for the DGEBA/D400 composites.

SEM micrographs of the composite fracture surface shown in Fig. 10 clearly illustrate that there is no agglomeration of the Al_2O_3. In addition, the Al_2O_3 particles are raised and debonded from the epoxy, without noticeable epoxy residue on the filler surface, suggesting that the fracture occurs at the epoxy–alumina interface. This weak adhesion can explain in part the lack of dependence of the composite properties on the particle shape, size, and size distribution. In general, the composite fracture behavior is substantially influenced by the particle–matrix adhesion [57,69]. However, typically, the particle surface treatment has a minor impact on the fracture toughness K_{1c}, and a large impact on the fracture strength and the appearance of the fracture surface [57,69]. Additional insight regarding the physical and chemical nature of the interfacial region would be valuable for understanding why failure occurs at the alumina–epoxy interface and what impact this might have on the composite toughness.

To investigate the epoxy–alumina interfacial chemistry, a synchrotron based surface science technique, NEXAFS, was utilized. In order to interpret the NEXAFS data shown in Fig. 12a and b it is important to understand how the data is plotted. An NEXAFS spectrum has three regions, including a pre-edge, a near-edge, and a post-edge region. The pre-edge region occurs before the absorption transition when the incident X-rays are adsorbed weakly by the sample (approximately 280, and 520 eV, respectively, for the carbon 1s and oxygen 1s transitions). The pre-edge region represents a background intensity that is subtracted from the spectra so that the pre-edge jump intensity is zero in these figures. In the near-edge region (approximately 285–310 and 530–570 eV, respectively, for carbon 1s and oxygen 1s transitions), the electron yield intensity increases as the incident X-ray energy is absorbed strongly by the sample. The near-edge region contains peaks that represent transitions associated with the specific types of chemical bonds present in the system. After the pre-edge background is subtracted, the intensity in the post-edge region (approximately 310 eV or greater, and 570 eV or greater, respectively, for the carbon 1s and oxygen 1s transitions) represents the total amount of carbon or oxygen in the sampling volume. In many cases the post-edge jump intensity can provide valuable information about the relative fractions of carbon or oxygen in a sample. However, many variables can impact the post-edge jump intensity including sample orientation, surface roughness, and the incident X-ray footprint on the sample, which is in part related to the angle of the incident energy relative to the surface. The NEXAFS spectra in Fig. 12 were measured at the magic angle to remove orientation dependency. If the fracture surfaces were perfectly planar and all had the same surface roughness, then quantitative analysis of the edge jump intensity would be prudent. However, the fracture does not occur in the exact same path for each sample during SENB testing. In addition, each sample was mounted in the NEXAFS instrument at a slightly variable angle. Therefore, the incident X-ray footprint is different for each sample. In addition, the fracture surfaces have different roughness, which depends on the filler loading. Due to these complications, the edge jump intensity is not quantitative for these specimens. Therefore, we normalized each spectrum with the intensity at either 315 or 570 eV, respectively, for the carbon 1s and oxygen 1s transitions, leaving a normalized edge jump intensity of 1. This removes the impact of the total amount of atoms sampled, which can vary due to the factors described above. Therefore changes in the peak intensities in the near-edge region represent changes in the sample chemistry if the spectra are both pre- and post-edge jump normalized. The spectra in Fig. 12a and b were both pre- and post-edge jump normalized.

The first step is to verify that the fracture propagates at the epoxy–alumina interface in support of the SEM images. Fig. 12a shows the oxygen 1s NEXAFS data for the unfilled DGEBA/D230 epoxy resin, the pure alumina, and a DGEBA/D230 composite with 50 vol.% alumina loading. A key point is that the oxygen signal from the unfilled epoxy and the alumina is different. A second point is that the composite with 50 vol.% alumina exhibits a clear contribution from the alumina oxygen spectrum. Since the probing depth of the oxygen signal is approximately 6 nm, the observation of an oxygen signal from the alumina in the composite verifies that the fracture occurs very near the alumina interface, as even a few monolayers of adsorbed epoxy on the alumina would attenuate the

alumina oxygen signal. In addition, a faint alumina oxygen contribution was even observed in the composites with 10% alumina loading.

Since both the SEM images and the NEXAFS data indicate that the fracture occurs within a few monolayers of the alumina interface, the carbon 1s NEXAFS spectra can be utilized to characterize the interfacial resin chemistry. The carbon 1s signal includes contributions from both the interfacial region (fracture surface near filler particles) and the bulk resin (fracture surface in regions where no filler was present). While the carbon 1s signal is not exclusively interfacial, the contribution from the interfacial region will increase with increasing filler loading, since the fracture occurs near the alumina substrate. Therefore, a difference between the interfacial resin composition and the bulk composition would result in a gradual change in the carbon 1s NEXAFS spectra with increased filler loading. Fig. 12b shows carbon 1s data of the fracture surfaces for DGEBA/D230 composites with filler loadings ranging from 0 to 50 vol.%. The carbon 1s spectra are independent of the filler loading. This indicates that the chemical composition at the alumina–epoxy interface is identical to the bulk resin composition. One potential issue with filled composites is preferential segregation of one of the resin monomers to the filler surface. This can lead to off-stoichiometric cures in that interfacial region. An off-stoichiometric cure in crosslinked polymers results in a polymer with a lower crosslink density and leads to a lower resin glass transition temperature and shear storage modulus. In addition, many other properties like the coefficients of thermal expansion and fracture resistance can be impacted by the resin stoichiometry. For these epoxy–alumina composites the carbon NEXAFS shows that preferential segregation of either the amine or the epoxy monomers to the alumina interface does not occur.

The epoxy monomer, DGEBA, exhibits a strong C1s $\rightarrow \pi^*_{C=C}$ transition in the carbon NEXAFS spectra near 285 eV (the arrow in Fig. 12b), due to the aromatic rings. The D230 amine hardener contains no such transition. Therefore, since the interfacial chemistry is being probed, preferential segregation of either the amine or the DGEBA monomer to the alumina surface would lead to a gradual decrease or increase, respectively, in this C1s $\rightarrow \pi^*_{C=C}$ signal from the fracture surface as the filler loading increases. Fig. 12b clearly shows a constant C1s $\rightarrow \pi^*_{C=C}$ peak area, illustrating that no preferential segregation occurs. The difference between the lowest and highest values of the C1s $\rightarrow \pi^*_{C=C}$ signal in Fig. 12b is 7%, with most spectra having an intensity near 1.9. No gradual trend was observed with filler loading and the data were scattered around this value. The carbon 1s spectra in Fig. 12b were both pre- and post-edge jump normalized. In identically planar surfaces, with the same surface roughness, it would be expected that the carbon edge jump intensity would decrease with increasing filler loading, if the fracture occurs at the epoxy–alumina interface. For these samples, however, the edge jump intensity was scattered with no trend as a function of filler loading. As was mentioned above this is from the varying and random X-ray footprint on the sample, due to the uneven fracture surfaces and difficulties in perfect sample mounting, coupled with differences in surface roughness with increasing filler loading. In addition, we cut the samples near the fracture surface to mount in the NEXAFS sample holder. Imperfect cutting contributed to the random X-ray footprint. Therefore, only the post-edge jump normalized spectra are quantitative. The strong oxygen signal from the alumina illustrates that the fracture occurs within a few nanometers of the epoxy–alumina interface. Since the fracture occurs at or within a few nanometers of the interface, the carbon signal can be utilized to investigate this interfacial chemistry. The independence of the pre- and post-edge jump normalized carbon 1s NEXAFS spectra with filler loading shows that the epoxy interfacial composition is the same as the bulk resin composition.

The combination of the oxygen and carbon NEXAFS experiments on the fracture surfaces for these composites illustrates two things. First, the fracture propagates within a few monolayers of the alumina–epoxy interface. Second, the interfacial resin composition is the same as the bulk composition. This is important for interpreting the fracture data in these composites. Since the interfacial composition is the same as the bulk, it is likely that the thermal, mechanical, and fracture properties of the interfacial region in these composite are similar to the bulk epoxy. While solid interfaces can certainly perturb the polymeric properties in the vicinity of the interface, with crosslinked systems, the first order effect that dominates the resin properties is the crosslink density. Since the interfacial stoichiometry is the same as the bulk stoichiometry, the interfacial and bulk resin crosslink density are also the same. Making these assumptions, the easiest path for a crack to propagate would be a path containing few or no covalent bonds present. Therefore, a reasonable conclusion is that the epoxy–alumina interface has less fracture resistance than the bulk resin due to either a lack of covalent bonding between the resin and the filler or a substantially smaller number of covalent bonds. Therefore, we hypothesize that a surface treatment for these alumina composites that leads to covalent epoxy–alumina bonding will improve the mechanical and fracture performances. More research is required with a broader range of filler surface treatments, particle sizes, particle–particle interactions, and resin crosslink densities to fully understand the impact of particle–matrix bonding on the composite properties.

In these experiments it was demonstrated that the epoxy–alumina composites are a robust system, and fairly large changes in particle shape, size, size distribution, filler loading, and resin crosslink density can be tolerated without a substantial change in thermal, mechanical, and fracture properties. Composite characterization coupled with SEM and NEXAFS analyses of the fracture surfaces indicated a weak epoxy–alumina interface, which we propose causes the insensitivity of the composite properties to change in the alumina properties. The particle size range explored with this study was an order of magnitude from approximately 2 to 20 μm. The particle shape ranged from nominally spherical to angular particulates. The reason that this size and shape range were chosen is because of the broad utility of these size and shape particles in practical applications such as high voltage stand-off, device encapsulation, flip-chip underfill technology, and dental restoratives.

Therefore these results are broadly applicable to a variety of academic and commercial sectors that would be concerned about material specifications, and variations in incoming material properties.

It is also pertinent to discuss the potential generality of these results to a broader range of particle sizes. We have labeled the epoxy–alumina interaction as weak. First, it is important to discuss our definition of a weak interface. We define a weak interface as one with little or no covalent bonding between the particle and the resin. However, there is a lower limit to this definition. The epoxy–alumina interface is not extremely weak. For example, no evidence of substantial interfacial slippage is observed. The epoxy at the alumina interface is not behaving as a free surface. Intimate contact exists between the epoxy and the alumina due to resin shrinkage during cure and cooling. There are also likely weak favorable attractive forces between the epoxy and the alumina such as van der Waals attractions, and potentially a small amount of hydrogen bonding between the alumina surface hydroxyls and the cured epoxy. The extent of particle–polymer hydrogen bonding is definitely small due to the dry nature of the alumina surface, as thermogravimetric analysis illustrated imperceptible mass loss with the Sumitomo particles and small mass loss with Alcoa T60. These weak attractive forces, combined with intimate particle–polymer contact do enable stress transfer, which explains the consistent increase in modulus with filler loading and the rule of mixtures' CTE behavior. However, the interaction is not strong enough to facilitate a resin composition change near the filler surface, to generate a T_g change in the composite, or to promote cohesive failure in the resin during crack propagation.

Given this definition of the strength of the alumina–epoxy interfacial interactions, it is now possible to speculate about the generality of these results for an expanded range of particle sizes. The insensitivity of the composite properties to filler size likely extends to larger particle sizes of approximately 100 to several hundred microns. Since the alumina–epoxy interaction is not extremely weak (as defined above) stress would still be transferred across the interface leading to an improvement in composite stiffness with particles in this size range. In addition, crack pinning phenomena would likely still be an important mechanism for the resistance to crack propagation with fillers of this length scale. For extremely large filler particles (in the order of millimeters or larger), the general results of this paper may not hold true. With a weak, non-covalently bound interface coupled with large particle sizes, the fracture behavior could be dominated by catastrophic interfacial failure, with little or no deformation in the polymer matrix. This has been observed in high explosives with high loadings of large particulates [84]. The result would be a more brittle composite material with a lower fracture resistance.

The insensitivity of the composite properties to particle size also likely extends well into the sub-micron regime (100 nm to 1 μm), due to the weak epoxy–alumina interface. For crosslinked polymers a critical length scale is the molecular weight between crosslinks (M_c), which is approximately 20–30 Å for the DGEBA/D230 and DGEBA/D400 resins. While weakly favorable interactions likely occur between the epoxy and the alumina particles, these are unlikely to perturb the polymer structure by more than a few M_c, particularly with the absence of preferential monomer segregation in these composites. Therefore a reasonable estimate for the thickness of the interfacial polymer (where the interfacial thermal and mechanical properties of the interface might change simply due to the interaction of the resin with the filler surface even in the absence of preferential monomer segregation) is 50 Å for these composites. For 2 μm diameter particles with a 5 nm interfacial region of polymer, the fraction of polymer that is interfacial is approximately 1.5% at 50 vol.% filler loading. At the same loading, with 200 nm particles the fraction of interfacial polymer is 15% given the same assumptions. Therefore, if the alumina substrate does induce an interfacial region in the crosslinked polymer then changes in composite thermal and mechanical properties might only be expected at high filler loadings as the particle size approaches 100 nm and below. Due to the enhanced surface area with particles approaching 100 nm, improved composite stiffness might start to be observed with these size particles, even with weak favorable epoxy–alumina interactions.

The impact of sub-micron particle loading on fracture toughness is not clear. Assuming the validity of the crack pinning model with regards to the fracture behavior of polymer composites, it might be expected that the fracture toughness would increase with the increasing number of particles at a particular filler volume fraction loading. This would be true with a strong interfacial bond that enables full matrix deformation upon crack pinning. However, with a weak interface like these epoxy–alumina composites in this study, we speculate that the enhanced surface area, having less fracture resistance than the bulk matrix, would counter balance the positive benefit of increasing particle numbers. One major challenge with particles in the sub-micron to nanometer size regime is particulate dispersion in the matrix. For the alumina–epoxy composites in this study, 5 μm particles are easily dispersed at 50 vol.% loading with a processable viscosity. Particles with 2 μm size are less easily dispersed at 50 vol.% loading. However, 500 nm particles at 30 vol.% loading in the epoxy gave an unprocessable paste with our mixing procedure. Particulate agglomeration and poor particle–resin wetting with sub-micron and nanoparticulates would likely degrade mechanical and fracture performances.

Certainly nanoparticulate-filled composites offer the potential for enhanced composite properties at low filler volume fractions, leading to lighter weight materials. However, the impact of nanoparticles on the composite properties is even less well understood, making predictions from the research on these alumina–epoxy composites difficult. A primary advantage of nanoparticles is the high surface area-to-volume ratio for the nanoparticle compared to the micron-sized version [85,86]. For linear polymers, as the particle size approaches the radius of gyration, R_g, dramatic changes in the polymeric properties such as stiffness, CTE, T_g, flow properties, etc. might be expected. Recent computational work has shown that as the filler size approaches R_g, even weak polymer–filler adsorption interactions in the order of kT can explain some of

the interesting rheological observations with nanofiller loaded composites, such as the high shear viscosity, enhanced shear thinning behavior, and solid-like behavior at low frequency [91]. A typical thermoplastic has an R_g near 4–10 nm. Therefore particle sizes approaching the dimensions of several tens of nanometers might induce these changes. For a crosslinked polymer like the epoxy resins in this study the critical length scale is the molecular weight between crosslinks (M_c), which is approximately 20–30 Å for these resins and even smaller than the R_g of a typical thermoplastic. Therefore the particle size required to induce dramatic changes in resin properties might be even smaller for a crosslinked system, with a small M_c. As with sub-micron particulates, dispersion of the nanoparticles in the matrix is difficult.

With nanocomposites in glassy polymers, particle agglomeration could degrade the potential benefits of the enhanced surface area. For example in nanoclay loaded epoxy resins, complete exfoliation of the nanoplatelets led to the highest storage modulus, but incomplete exfoliation led to lower modulus values [87]. With alumina and magnetite nanoparticles in polystyrene and polymethylmethacrylate composites, a subtle decrease in the materials' stiffness was observed and was attributed to a weak polymer–filler interaction and a less dense interfacial region, as opposed to particulate agglomeration [88]. With silica nanofillers in polyamide-6, the shear modulus enhancements in the glassy region were similar to those with micron filler loadings and could be predicted with Kerner's equation [89]. With regards to the fracture behavior of nanocomposites, even if the nanoparticles are intimately dispersed without agglomeration, an interesting and pertinent question is whether a nanoparticle can deflect or deform an advancing crack tip, which might typically have a radius in the order of a micron. Extremely small nanoparticles might not effectively ''pin'' a crack, regardless of the strength of the particle–polymer interaction. Therefore, the potential benefits of the nanoparticle loading on fracture might be solely due to the enhanced amount of interfacial region where the polymer properties are modified in the presence of the nanoparticle surface. In addition, the specific mechanisms of failure in polymer nanocomposites are not well understood. For example, simulations have shown that nanofillers improve the composite toughness by the energy dissipation associated with the mobility of the nanoparticle [90]. Clearly more research is required to investigate nanoparticle loaded composite.

4. Summary

Alumina filled epoxy composites were studied as a model system. The variables tested included the particle shape, size, size distribution, filler loading, and resin crosslink density. The primary observations of this paper are:

(a) the epoxy–alumina composites are a robust materials system and fairly large changes in particle shape, size, and size distribution can be tolerated without causing a substantial change in the thermal and mechanical properties or fracture toughness of the system. This is likely due to a weak epoxy–alumina interaction.
(b) Filler loading and resin crosslink density were the critical variables that caused changes in the cured composite properties. However, large changes in the filler loading or crosslink density are required to impart a substantial change in properties, further illustrating the robust nature of these composites.
(c) The epoxy–alumina interface is weak with little or no covalent bonding present. The composite T_g did not change with filler loading, and the rubbery CTE did not deviate from rule of mixtures' behavior. These both indicated a weak polymer–substrate interaction. In addition, SEM coupled with NEXAFS characterization of the fracture surfaces showed that crack propagation occurs at the epoxy–alumina interface, with little or no residual polymer adsorbed to the alumina particles. NEXAFS also showed that the interfacial epoxy composition is the same as the bulk polymer. Therefore, variations in the interfacial resin properties, due to preferential monomer segregation to the alumina surface, plays no role in these composites.
(d) The epoxy crosslink density had some interesting subtle effects on the mechanical properties of the alumina filled composites. In particular, the shear storage modulus–temperature profile exhibited a subtle broadening in the glass transition region and at temperatures slightly above the T_g, with increased filler loading. The broadening was more pronounced in the lower crosslink density resin. Due to the weak epoxy–alumina interface, we conclude that this effect is likely due to particle–particle contacts that increase with increasing filler loading.
(e) The resin crosslink density can impact the fracture toughness in the composite even if a change in the unfilled resin toughness is not observed. In particular, the DGEBA/D400 composites exhibited higher fracture toughness than the DGEBA/D230 composites despite the similar fracture toughness of the unfilled resin and despite the measurement being made at the same temperature relative to the composite T_g.
(f) Traditional wisdom is supported. When this data are compared with existing literature, it is clear that the incorporation of filler into an epoxy matrix is more effective at improving the relative fracture toughness in composites with resins that exhibit a lower initial unfilled matrix toughness.

Acknowledgements

Sandia National Laboratories (Albuquerque, NM) provided financial support. Sandia is a multiprogram laboratory operated by Sandia Corporation, a Lockheed Martin Company, for the United States Department of Energy under Contract No. DE-AC04-94AL85000.

References

[1] Lee H, Neville K. Handbook of epoxy resins. New York: McGraw-Hill; 1967.

[2] Nakamura Y, Yamaguchi M, Okubo M, Matsumoto T. J Appl Polym Sci 1992;45:1281–9.
[3] Okazaki M, Murota M, Kawaguchi Y, Tsubokawa N. J Appl Polym Sci 2001;80:573–9.
[4] Wetzel B, Haupert F, Zhang MQ. Compos Sci Technol 2003;63(14): 2055–67.
[5] Zeey RH, Huang YH, Chen JJ, Jang BZ. Polym Compos 1989; 10(4):205–14.
[6] Kim DJ, Kang PH, Nho YC. J Appl Polym Sci 2004;91:1898–903.
[7] Arayasantiparb D, McKnight S, Libera M. J Adhes Sci Technol 2001;15(12):1463–84.
[8] Hawley GC. In: Milewski JV, Katz HS, editors. Handbook of reinforcements for plastics. New York: Van Nostrand Reinhold Company; 1987.
[9] Maiti SN, Sharma KK. J Mater Sci 1992;27:4605.
[10] Nielsen LE, Landel RF. Mechanical properties of polymers and composites. 2nd ed. New York: Marcel Dekker, Inc; 1994.
[11] Rothon R, editor. Particulate-filled polymer composites. London: Longman Scientific and Technical; 1995.
[12] Mamunya YP, Davydenko VV, Pissis P, Lebedev EV. Eur Polym J 2002;38:1887.
[13] Wong CP, Bollampalla RS. J Appl Polym Sci 1999;74:3396.
[14] Rothon RN. Adv Polym Sci 1999;139:67–107.
[15] Rothon RN. Flame Retard 1997;90:156.
[16] Zhang Z, Wong CP. IEEE Trans Adv Packag 2003;26(2):199–205.
[17] Babbington DA, Enos J, Cox JMark, Barron J. Mod Plast 1987;64(8):72, 74, 76.
[18] Craig RG, editor. Restorative dental materials. 10th ed. St. Louis: Mosby-Year Book, Inc; 1997.
[19] Stannard JG. Materials in dentistry. 2nd ed. Hanover: Denali Pub; 1988.
[20] Madenci E, Shkarayev S, Mahajan R. Trans ASME J Elect Pack 1998; 120(4):336–41.
[21] Wu TY, Tsukada Y, Chen WT. Proc Electron Comp Technol Conf 1996:524–34.
[22] Voa HT, Todd M, Shia FG, Shapiroa AA, Edwards M. Microelectron J 2001;32(4):331–8.
[23] Yee AF, Pearson RA. J Mater Sci 1986;21:2462–74.
[24] Sankaran S, Chanda M. J Appl Polym Sci 1990;39(8):1635–47.
[25] Certain commercial equipment, instruments, or materials are identified in this paper in order to specify the experimental procedure adequately. Such identification is not intended to imply recommendation or endorsement by the National Institute of Standards and Technology, nor it is intended to imply that the materials or equipment identified is necessarily the best available for the purpose.
[26] For detailed information about the NIST/Dow Soft X-ray Materials Characterization Facility at NSLS BNL, see: <http://www.nsls.bnl.gov/beamlines/beamline.asp?blid=U7A>.
[27] Stöhr J. NEXAFS spectroscopy. In: Springer series in surface science, vol. 25. Heidelberg: Springer; 1992.
[28] Goyanes SN, König PG, Marconi JD. J Appl Polym Sci 2003;88(4): 883–92.
[29] Kawana S, Jones RAL. Phys Rev E 2001;63:021501-1.
[30] Lenhart JL, Wu WL. Macromolecules 2002;35:5145.
[31] Lenhart JL, Wu WL. Langmuir 2003;19:4863.
[32] Reiter G. Europhys Lett 1993;23(8):579.
[33] Reiter G. Macromolecules 1994;27:3046.
[34] Orts WJ, van Zanten JH, Wu W-L, Satija SK. Phys Rev Lett 1993;71:867.
[35] Fryer DS, Nealey PF, de Pablo JJ. Macromolecules 2000;33:6439.
[36] Keddie JL, Jones RA, Cory RA. Faraday Discuss 1994;98:219.
[37] Tate RS, Fryer DS, Pasqualini S, Montague MF, de Pablo JJ, Nealey PF. J Chem Phys 2001;115:9982.
[38] Wallace WE, van Zanten JH, Wu WL. Phys Rev E 1995;52:R3329.
[39] Fryer DS, Peters RD, Kim EJ, Tomaszewski JE, de Pablo JJ, Nealey PF, et al. Macromolecules 2001;34:5627.
[40] van Zanten JH, Wallace WE, Wu WL. Phys Rev E 1996;53:R2053.
[41] Starr FW, Schroder TB, Glotzer SC. Phys Rev E 2001;64:021802.
[42] Wu W-L, van Zanten JH, Orts WJ. Macromolecules 1995;28:771.
[43] Tsui OKC, Zhang HF. Macromolecules 2001;34:9139.
[44] Tsui OKC, Russell TP, Hawker CJ. Macromolecules 2001;34:5535.
[45] Forrest JA, Dalnokin-Veress K, Stevens JR, Dutcher JR. Phys Rev Lett 1996;77:2002.
[46] Prucker O, Christian S, Bock H, Ruhe J, Frank CW, Knoll W. Macromol Chem Phys 1998;199:1435.
[47] Fakao K, Miyamoto Y. Phys Rev E 2000;61:1743.
[48] Keddie JL, Jones RAL, Cory RA. Europhys Lett 1994;27:59.
[49] Soles C, Lin EK, Lenhart JL, Jones RL, Wu W-L, Goldfarb DL, et al. J Vac Sci Technol B 2001;19:2690.
[50] Pochan DJ, Lin EK, Satija SK, Wu W-L. Macromolecules 2001;34:3041.
[51] Ash BJ, Siegel RW, Schadler LS. J Polym Sci Part B Polym Phys 2004; 42(23):4371–83.
[52] Vassileva E, Friedrich K. J Appl Polym Sci 2003;89:3774.
[53] Ishai O, Cohen LJ. Int J Mech Sci 1967;9:539–46.
[54] Sahu S, Broutman LJ. Polym Eng Sci 1972;12(2):91–100.
[55] Mallick PK, Broutman LJ. Mater Sci Eng 1975;18:63–73.
[56] Young RJ, Beaumont PWR. J Mater Sci 1977;12(4):684–92.
[57] Spanoudakis J, Young RJ. J Mater Sci 1984;19(2):473–86.
[58] Nakamura Y, Yamaguchi M, Okubo M, Matsumoto T. J Appl Polym Sci 1993;44:151.
[59] Gent AN. J Mater Sci 1980;15(11):2884–8.
[60] Alter H. J Appl Polym Sci 1965;9(4):1525–31.
[61] Warrick EL, Lauterbur PC. Ind Eng Chem 1955;47:486–91.
[62] Lewis TB, Nielsen LE. J Appl Polym Sci 1970;14:1449.
[63] Vollenberg PHT, Heikens D. Polymer 1989;30(9):1656–62.
[64] Crawford E, Lesser AJ. J Polym Sci Part B Polym Phys 1998;36:1371.
[65] Kwak GH, Park SJ, Lee JR. J Appl Polym Sci 2000;78(2):290–7.
[66] Einstein A. Ann Phys 1906;19:289.
[67] Guth E. J Appl Phys 1945;16:20.
[68] Lee J, Yee AF. J Appl Polym Sci 2001;79:1371.
[69] Moloney AC, Kausch HH, Kaiser T, Beer HR. J Mater Sci 1987;22:381.
[70] Nakamura Y, Yamaguchi M, Kitayama A, Okubo M, Matsumoto T. Polymer 1991;32:2221.
[71] Nakamura Y, Yamaguchi M, Okubo M, Matsumoto T. Polymer 1992;33:3415.
[72] Kinloch AJ, Maxwell DL, Young RJ. J Mater Sci 1985;20(11):4169–84.
[73] Lee J, Yee AF. Polymer 2000;41(23):8375–85.
[74] Kinloch AJ, Young RJ. Fracture behavior in polymers. London: Chapman and Hall; 1983.
[75] Moloney AC, Kausch HH, Stieger HR. J Mater Sci 1983;18:208.
[76] Lange FF. Philos Mag 1970;22(179):983–92.
[77] Evans AG. Philos Mag 1972;26(6):1327–44.
[78] Lange FF, Radford KC. J Mater Sci 1971;6(9):1197–203.
[79] Lange FF. J Am Ceram Soc 1971;54:614–20.
[80] Green DJ, Nicholson PS, Embury JD. J Mater Sci 1979;14(6):1413–20.
[81] Green DJ, Nicholson PS, Embury JD. J Mater Sci 1979;14(7):1657–61.
[82] Kawaguchi T, Pearson RA. Polymer 2003;44:4239–47.
[83] Moloney AC, Kausch HH, Stieger HR. J Mater Sci 1984;19:1125–30.
[84] Tan H, Huang Y, Liu C, Geubelle PH. Int J Plast 2005;21:1890–918.
[85] Winey KI, Vaia RA. MRS Bull 2007;32:314–22.
[86] Schadler LS, Kumar SK, Benicewicz BC, Lewis SL, Harton SE. MRS Bull 2007;32:335–40.
[87] Miyagawa H, Drzal LT. J Adhes Sci Technol 2004;18:1571–88.
[88] Ciprari D, Jacob K, Tannenbaum R. Macromolecules 2006;39: 6565–73.
[89] Reynaud E, Jouen T, Gauthier C, Vigier G, Varlet J. Polymer 2001; 42:8759–68.
[90] Gersappe D. Phys Rev Lett 2002;89:058301-1–4.
[91] Sarvestani AS, Jabbari E. Macromol Theory Simul 2007;16:378–85.